

Explicit filtering for large eddy simulation as use of a spectral buffer

Joseph Mathew*

Department of Aerospace Engineering, Indian Institute of Science, Bangalore 560012, India

Abstract

The explicit filtering method for large eddy simulation (LES), which comprises integration of the governing equations without any added terms for sub-grid-scale modeling and the application of a low-pass filter to transported fields, is discussed. The shapes of filter response functions of numerical schemes for spatial derivatives and the explicit filter, that have been used for several LES, are examined. Generally, these are flat (no filtering) over a range of low wavenumbers, and then fall off over a small range of the highest represented wavenumbers. It is argued that this high wavenumber part can be viewed as a spectral buffer analogous to physical buffer (or sponge) zones used near outflow boundaries. The monotonic convergence of this approach to a direct numerical simulation, and the shifting of the spectral buffer to larger wavenumbers as the represented spectral range is increased, without altering the low wavenumber part of solutions, is demonstrated with LES of two sample flows. Connections to other widely used methods—the Smagorinsky model, MILES and another ILES—are also explained.

Keywords: Turbulent flow, Large eddy simulation modeling

1. Introduction

Large eddy simulation (LES) connotes a numerical simulation that is restricted to a range of the largest scales of a turbulent flow. The approximation is useful when the solution is qualitatively correct, and typical quantities of interest, such as flow statistics, are obtained with acceptable accuracy. The error is acceptable because of the great reduction in computing effort (grid size, computation time) compared with that required for a solution that contains all dynamically significant scales. There have been many reports of LES by various techniques that have been developed to overcome shortfalls of various approaches. A comprehensive presentation of techniques and sample results can be found in Sagaut [1]. Much of the effort had been directed at finding the best sub-grid-scale (SGS) model which must capture the effect of the omitted small scales on the computed large scales. It cannot be said that any one approach has emerged as a sole best method. Instead, practitioners adopt a particular method (numerical scheme and SGS model) which has proved successful for their studies, and whose requirements for each class of flows (free shear flows, wall-bounded flows) are known from experience. This paper discusses some new understanding of an explicit filtering approach introduced in Mathew et al. [2], and connections to other popular methods. In the literature, explicit filtering can also refer to filtering nonlinear terms alone, which has been examined by Lund [3]. It was considered a means of controlling numerical error and not as an SGS model, unlike the model discussed here.

The derivation of the explicit filtering SGS model is described below. Next, its application to turbulent flows with two kinds of numerical scheme-filter pairs is discussed. The shapes of the filter response functions motivates the idea of a spectral buffer. Two examples show the presence of this buffer at different grid resolutions, filter cut-offs, and Reynolds numbers. Connections to other SGS models are discussed in § 4.

1.1. Approximate deconvolution model

The explicit filtering method of Mathew et al. [2] was derived from the approximate deconvolution model (ADM) [4]. Salient aspects will be summarized below for completeness. Consider the one-dimensional evolution equation for

*Corresponding author

Email address: joseph@aero.iisc.ernet.in (Joseph Mathew)

$u(x, t)$,

$$\frac{\partial u}{\partial t} + \frac{\partial}{\partial x} f(u) = 0, \quad (1)$$

where $f(u)$ is a nonlinear function. An LES can be interpreted as either obtaining an approximation $\bar{u}(x, t)$ that contains a large scale part of $u(x, t)$, or the approximation that can be obtained on a coarse grid which implicitly limits the range of wavenumbers in the solution. Then $\bar{u} = G * u = \int G(x - x') u(x') dx$, where G is a low pass filter. The evolution equation for $\bar{u}(x, t)$ is obtained by applying the filter to eqn. (1) to get

$$\frac{\partial \bar{u}}{\partial t} + G * \frac{\partial}{\partial x} f(u) = 0. \quad (2)$$

Equation (2) can be written in the form of the original equation with a remainder \mathcal{R}

$$\begin{aligned} \frac{\partial \bar{u}}{\partial t} + \frac{\partial}{\partial x} f(\bar{u}) &= \mathcal{R}, \\ \mathcal{R} &= \frac{\partial f(\bar{u})}{\partial x} - G * \frac{\partial f(u)}{\partial x}. \end{aligned} \quad (3)$$

$\mathcal{R} \equiv 0$ unless $f(u)$ is nonlinear. Since u is not known when solving for \bar{u} , \mathcal{R} must be replaced with a model $\mathcal{R}_m(\bar{u})$ for closure. In ADM [4]

$$\mathcal{R}_m = \frac{\partial f(\bar{u})}{\partial x} - G * \frac{\partial f(u^*)}{\partial x}, \quad (4)$$

where $u^*(x, t) = Q * \bar{u}$ is an approximation to $u(x, t)$ obtained by deconvolution of the filtered variable \bar{u} . The equation solved when using ADM is

$$\frac{\partial \bar{u}}{\partial t} + G * \frac{\partial f(Q * \bar{u})}{\partial x} = 0. \quad (5)$$

During the early development of ADM, when the method was applied to different types of problems, filters were obtained from implicit formulas (Padé-type, $G(\alpha)$ with different values of the filter parameter α ¹) and from explicit formulas [6]. The deconvolution $Q * \bar{u}$ was performed by applying the filter G several times as per an expansion of the operator Q in terms of G . In all cases, excellent results for LES were presented. Around the same time, Geurts [7] examined a similar de-filtering, taking the primary filter to be a top-hat function in physical space, and inversion to be exact for polynomials. It was not understood whether there was a best convolution/filter-deconvolution/defilter pair G and Q , or that all pairs that satisfied some property would be suitable. As will be shown below, the solution depends on the effective filter $E = Q * G$ rather than on the constituent filter and deconvolution operators themselves. Secondary filtering in ADM will be discussed later.

1.2. Explicit filtering implementation of ADM

The implementation of ADM by solving eqn. (5) involves the following steps to obtain $\bar{u}(x, t^{n+1})$ at the $n + 1$ timestep given $\bar{u}(x, t^n)$.

1. Deconvolution: $u^* = Q * \bar{u}(x, t^n)$
2. Integration of eqn. (5): $\bar{u}(x, t^n) \rightarrow \bar{u}(x, t^{n+1})$

This integration step by Euler forward is

$$\bar{u}(x, t^{n+1}) = \bar{u}(x, t^n) - \Delta t G * \frac{\partial f(u^*)}{\partial x},$$

and can be performed in two steps

$$a(x) = u^*(x, t^n) - \Delta t \frac{\partial f(u^*)}{\partial x} \quad (6)$$

$$\bar{u}(x, t^{n+1}) = G * a(x) + [\bar{u}(x, t^n) - G * u^*(x, t^n)] \quad (7)$$

¹ $\alpha = -0.2$ in ref. [5], $\alpha = 0.25$ in ref. [4].

The quantity within the square brackets in eqn. (7) is small and can be neglected because the essential requirement for the deconvolved field is that $u^* \approx u$ over a range of large scales; then $\bar{u} = G * u \approx G * u^*$. The intermediate field $a(x)$ can also be written as $u^*(x, t^{n+1})$. This alternate implementation comprises the following three steps:

1. Deconvolution: $u^*(x, t^n) = Q * \bar{u}(x, t^n)$
2. Integration of eqn. (1) with u^* instead of u : $u^*(x, t^n) \rightarrow u^*(x, t^{n+1})$ (applying equation 6)
3. Filtering: $\bar{u}(x, t^{n+1}) = G * u^*(x, t^{n+1})$ (applying equation 7)

Mathew et al. [2] observed that, with this latter form, the simulation proceeds by repeating the following two steps: an integration of the original evolution equation (1) followed by a filtering and deconvolution that can be combined into an (explicit) filtering of the evolving field with a resultant filter $E = G * Q$. Since Q is an approximate inverse of G over a range of low wavenumbers by definition, $E \approx I$ over that range of low wavenumbers. Beyond that range, we would like E to fall off to zero smoothly. In the standard ADM form (eqn. 5) it is not evident that the results depend on the effective filter E only. One could expect that G and Q could be varied independently.

2. Explicit filtering for LES of turbulent flow

For LES of a turbulent flow, eqn. 1 is replaced by the Navier-Stokes equations. For incompressible flow, the explicit filtering method described above can be implemented by integrating the momentum equation to obtain a velocity field, obtain the pressure field, and correct the velocity field so that it is divergence free as in a DNS. Next, an explicit filter E should be applied to this velocity field, since that is the transported field. For compressible flow, there are two other transport equations for, say, density and energy, and these fields would also be filtered. Other intermediate variables, like temperature or pressure, that appear in the equations needn't be filtered. Note also that it is not necessary to use filters that commute with differentiation, since commutation is not invoked at any stage in deriving this method.

When the momentum equation is written in terms of the LES field, the remainder \mathcal{R} is termed the SGS stress which requires an SGS model. SGS modeling can be classified broadly into structural and functional models [1]. A structural model is obtained by replacing the full-spectrum fields in SGS terms with an approximation obtained from the computable partial spectrum fields. ADM is an example that replaces the velocity field $\mathbf{u}(\mathbf{x}, t)$ with the approximation $\mathbf{u}^*(\mathbf{x}, t)$ that has been obtained by deconvolution of the LES field $\bar{\mathbf{u}}(\mathbf{x}, t)$. A velocity estimation model is another kind where an approximation to $\mathbf{u}(\mathbf{x}, t)$ is obtained by an integration of the governing equations (or an approximation that makes computations economical) with a slightly larger spectral content and for short durations [8]. An example of a functional model is the Smagorinsky model. A well-known feature of turbulent flow is the net transfer of energy from larger scales to smaller scales. In an LES where only a large scale part of the flow is computed, this energy transfer is prevented, causing a growth of high wavenumber content, the appearance of wiggles in physical space, and the solution diverges. The Smagorinsky model dissipates spectral content of all scales but increasingly at the highest wavenumbers. The coefficient controls the magnitude of dissipation, and when it is determined dynamically from the evolving fields themselves [9], the model has been found to be more useful.

A large number of studies have appeared that use the FDL3DI code which combines an explicit filtering step with high-resolution, compact difference schemes. The method was first described in Visbal and Gaitonde [10]. Examples of LES were reported subsequently [11]. Derivatives were computed with 4th and 6th-order compact differences and conserved variables were filtered with 8th and 10th-order Padé filters; there were no added SGS model terms in the equations that were solved. This approach is quite similar to those [2, 12] described above. The numerical scheme and the explicit filter have flat response functions with a smooth fall-off near the high wavenumber end. Bogey and Bailly [13] proposed high-order explicit difference schemes (8, 10 and 12th-order) with optimized coefficients that have good resolution characteristics like compact schemes. They also devised a selective filter with response functions similar to that shown in Fig. 1 (see Fig. 3 in their paper [13]). They have used this method for LES of round jets and computed turbulence profiles and the radiated sound.

2.1. Filter characteristics

Although derived as a structural model, the explicit filtering model of Mathew et al. [2] is a functional model. Before elaborating, let us consider examples of G , Q and $E = QG$. Let u_j denote values of the function on a uniform

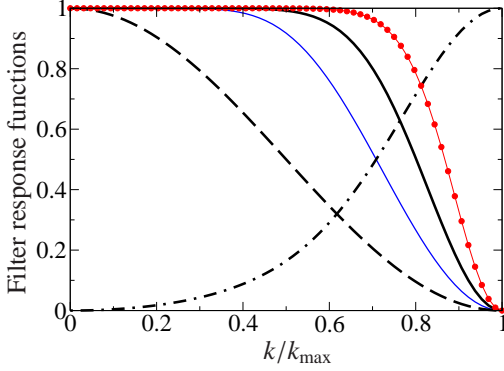


Figure 1: Filter response functions associated with Padé filter defined by eqn. 8. ---: $\hat{G}(k; \alpha = 0)$, - · - · -: $(\hat{Q}_{ADM}(k) - 1)/J; \alpha = 0, J = 5)$, —: $\hat{E}(k; \alpha = 0)$, —: $\hat{E}(k; \alpha = -0.2)$, - · - · -: $\hat{E}(k; \alpha = 0.2)$

grid of N points $x_j = jh$ ($j = 0, 1, \dots, N$). When combined with end-point formulas, the following implicit formula provides a filtered field \bar{u}_i

$$\alpha \bar{u}_{j-1} + \bar{u}_j + \alpha \bar{u}_{j+1} = \left(\alpha + \frac{1}{2} \right) \left(u_j + \frac{1}{2} (u_{j-1} + u_{j+1}) \right). \quad (8)$$

The sole free parameter α controls the shape of the filter response function. We write $\bar{u} = G * u$. For simplicity, suppose u to be periodic, with period 2π . Then, Fourier coefficients of wavenumber k are related as $\hat{\bar{u}}(k) = \hat{G}(k) \hat{u}(k)$, where variables with carets are coefficients of the appropriate Fourier series. Figure 1 shows $\hat{G}(k)$ with $\alpha = 0$. Note that there is significant filtering at all wavenumbers. Owing to the restriction of the function u to the grid of N intervals, the spectral content of the filtered field is restricted to $0 \leq k \leq k_{\max}$ and $k_{\max} = N/2$. An exact inverse is not possible because content with $k > N/2$ is not available. An obvious approximate inverse is

$$\hat{G}_N^{-1} = \begin{cases} 1/\hat{G} & (0 \leq k < N/2) \\ 0 & (k = N/2) \end{cases}$$

Formally then, the deconvolution filter $Q = G_N^{-1}$. The explicit filter $\hat{E} = \hat{G} \hat{Q} = 1$ ($0 \leq k < N/2$) and vanishes for $k = N/2$. LES with these filters amounts to integrating the transport equation without any explicit filtering. The explicit filtering SGS model is then inactive, will prove inadequate, and the code will diverge, *unless* the filtering due to *other* operations such as numerical differentiation provide the expected functionality.

The approximate deconvolution operator proposed by Stolz and Adams [4] is the truncated series

$$Q_{ADM} = \sum_{j=0}^J (I - G)^j$$

where I is the identity operator. Figure 1 shows the filter response function for $\hat{Q}_{ADM}(\alpha = 0)$ when 6 terms in the expansion are taken. Also shown are the implied explicit filters $\hat{E} = \hat{G} \hat{Q}_{ADM}$ for $\alpha = -0.2, 0, 0.2$. The explicit filter E is flat (no filtering) over a range of low wavenumbers and then falls smoothly to zero over a small part of the highest represented wavenumbers. As α increases the cut-off wavenumber k_{cutoff} increases. A suitable definition is of k_{cutoff} is that $\hat{E}(k_{\text{cutoff}}) = 0.9$.

LES by explicit filtering with filters E , with characteristics similar to those in Fig. 1, have proved to be successful. Another common feature of these successful simulations is that the numerical methods comprised either high-resolution, implicit (compact) difference or very high-order, explicit difference formulas that also provide high-resolution. Of course, this is understandable: difference formulas may be viewed as providing a spectrally-accurate derivative combined with low-pass filtering. The implied filter of a symmetric, implicit difference formula or a high-order explicit difference formula is nearly flat over a range of low wavenumbers and then falls off to zero. When such difference formulas are used the governing equations are integrated accurately over a range of low wavenumbers.

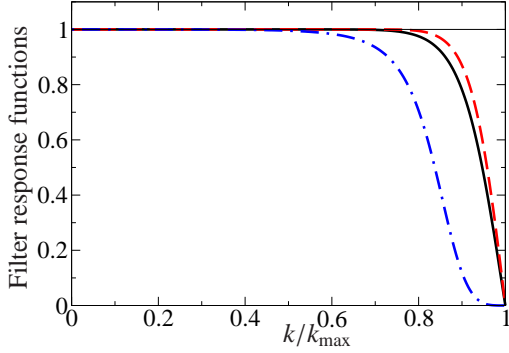


Figure 2: Filtering of formulas designed by Chakravorty [12]. —: first derivative; - - -: interpolation; - · - · -: explicit filter E .

Chakravorty [12] performed LES of incompressible and variable density (low-Mach number) flows using compact difference formulas. For the staggered grid algorithm, the needed interpolations were also performed using high-resolution, implicit formulas[14]. Filtering characteristics of all numerical procedures were designed to be flat over a range of low wavenumbers and to fall off at high wavenumbers, like the explicit filter E shown in Fig. 1. Five-point stencils were taken and constrained at two or three wavenumbers to design derivative and interpolation formulas with a large range of wavenumbers over which near-spectral accuracy would be obtained. Truncation error was 4th-order for all formulas. The explicit filter, defined on a 5-point stencil, has one free parameter and is 4th-order. The filter response functions for the 1st derivative, interpolation and the explicit filter are shown in Fig.2. Note that there is a clear separation between the cut-off wavenumbers of procedures in the numerical scheme and the explicit filter. The cut-off is at a smaller wavenumber for the explicit filter ($k_{\text{cutoff}} \approx 0.7k_{\text{max}}$). Below the cut-off, spectral accuracy is maintained. A similar relation between cut-offs of explicit filter and numerical scheme was used in Mathew et al. [2] for LES of supersonic channel flow.

The earlier papers [2, 15] had advocated that the cutoff wavenumber of the explicit filter be smaller than that of the numerical method. The operations in Chakravorty [12] have also followed this principle. However, it is not necessary because it is the combination that is effective in a simulation. For the LES of Visbal and Rizzetta [11], when the 10th-order filter is applied with a high value for the filter parameter of 0.49, the cut-off of the filter is very close to the maximum wavenumber and clearly larger than that of the derivative operations. We have a similar experience when using the MacCormack-type splitting scheme of Hixon and Turkel [16]. Figure 3 shows filtering characteristics of the standard 6th-order compact difference formula (eqn. (2.1.7) in Lele [17]), and a 10th-order Padé filter (filter F10 in table IV of Visbal and Rizzetta [11] with parameter $\alpha = 0.498$). The implied filter of the difference formula has a smaller cut-off than the optimized schemes shown in Fig. 2. So it has been sufficient to use a filter with a higher cut-off than that of the difference formula [18, 19]. This strategy has been used for the round jet simulations discussed in §3 below.

2.2. Explicit filtering as employing a spectral buffer

For simulations of unsteady, spatially developing flows, it is a widespread practice to have a buffer zone between the outflow boundary surface and the region of interest. Within the buffer zone the solution will not have the same accuracy as that in the region of interest. It may even be quite wrong. If the grid spacing in the buffer zone is increased aggressively, smaller scale motions that convect into the buffer zone become damped numerically because they can no longer be represented in coarse regions. Damping can also be effected by adding a term that takes the solution to a smoother profile. Then at the outflow boundary, a simple convective condition with a uniform convection velocity, or the more detailed treatment based on characteristics [20, 21] can be applied. In such cases there is an expectation that any significant error due to the buffer zone treatment will be restricted to the buffer zone, and to a smaller extent upstream of the buffer, to about the thickness of the outgoing shear layers.

Our studies with the explicit filtering method indicate that the result of filtering is like using a buffer zone in spectral space. The buffer zone spans a small range of the largest represented wavenumbers, and the corresponding

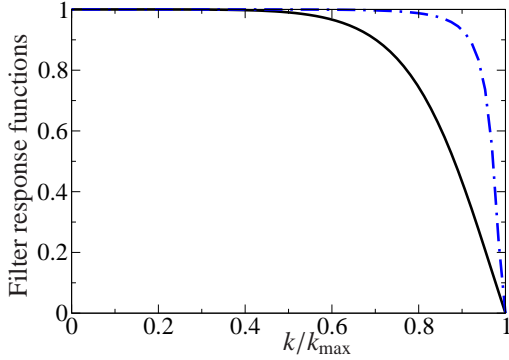


Figure 3: Filtering of standard 6th-order compact difference formula (—) and 10th-order filter F10 with $\alpha = 0.498$ (- · - · -).

range of represented high frequencies. Though these are small scale motions that are computed, the filtering damps the energy contained, smoothly and increasingly towards k_{\max} . The notion of a spectral buffer is suggested strongly by the shape of the filter response functions of the numerical schemes and the explicit filter. In all computations employing this approach, these functions have an essentially flat portion over a significant range of represented wavenumbers and a smooth fall-off. For the two kinds of computations represented in Figs. 2 and 3, the spectral buffer spans the approximate range $0.7 < k/k_{\max} < 1$. In this range, the numerical schemes have significant errors. Errors in the solution that would cause divergence begin to appear because the physical (and mathematical) requirement of energy transfer to smaller scales ($k > k_{\max}$) is not met on an LES grid. Explicit filtering with a high-resolution filter meets one part of this requirement that the energy be transferred out of this spectral range. Just as one is not concerned about what happens within and beyond a physical buffer layer, one should not be concerned about what happens within and beyond the spectral buffer. However, it is only when the response functions nearly flat characteristics over a range of low wavenumbers that there is a small spectral buffer zone. When low-order schemes are used, there is significant filtering even of low wavenumber content, making the method less efficient: a relatively finer grid is needed for the same level of accuracy over a fixed range of large scales. This is the functional modeling provided by explicit filtering as an SGS model, though it was derived as a structural model.

3. LES examples

When there is such a clear separation between cut-off wavenumbers of numerical scheme and explicit filter, it is possible to examine the LES obtained as the cut-off wavenumber of the explicit filter alone is changed. With LES of of supersonic channel flow Mathew et al. [2] have shown *monotonic* convergence towards the DNS solution as the LES grid was refined, or as filter cut-off was increased. Perhaps an even more compelling demonstration was obtained by Chakravorty [12] by performing several LES and a DNS of forced homogeneous, isotropic turbulence. Figure 4 shows the compensated energy spectrum as a function of wavenumber k scaled with the Kolmogorov length scale η . The DNS was on a grid of $192 \times 192 \times 192$ points. LES were conducted on grids of 32^3 , 48^3 , and 64^3 points, with four different values of cut-off wavenumbers of the explicit filter. Clearly, a) LES solutions converge monotonically to the DNS with grid refinement or when filter cutoff is increased on a given grid, and b) the changes are to high wavenumber content only. As grid size increases there is essentially no change to low wavenumber content even as the spectral range increases. If one compares any one of the LES, say, on the 32^3 grid and with the smallest filter cut-off, with the DNS, one infers that the explicit filtering is providing a spectral buffer beyond scaled wavelength $k\eta \approx 0.1$. The fall-off of the spectrum is due to the filter since the numerical differentiation is spectrally accurate over a larger range. On a given grid, as the filter cutoff wavenumber is increased, the spectral buffer zone becomes thinner. Solutions on different grids demonstrate a complementary feature: on a finer grid, the buffer zone has moved to a range of larger wavenumbers. Significant errors remain confined to this buffer zone. While it not *a priori* evident that errors would be confined to wavenumbers larger than the scheme cutoff, these results show no significant contamination of smaller wavenumber content.

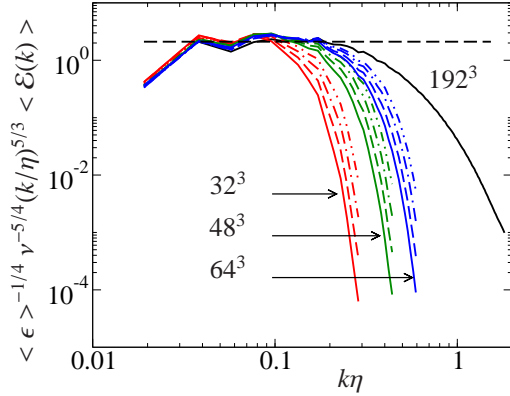


Figure 4: Compensated energy spectrum from forced homogeneous, isotropic turbulence simulations of Chakravorty [12]. LES grid sizes are 32^3 , 48^3 and 64^3 , and DNS is with 192^3 points. For each group of LES there are 4 curves corresponding to simulations with 4 filter cutoff values.

case	Re	L_x/D	$L_y/D, L_z/D$	N_x	N_y, N_z	B_u
A	11×10^3	30	10	263	253	6.01
B	11×10^3	70	40	426	473	5.92
C	1.1×10^6	30	10	263	253	7.04
D	1.1×10^6	30	10	406	387	5.88

Table 1: Round jet simulation parameters

A second example is that of spatially developing, compressible round jets at very high Reynolds numbers. Simulation parameters are listed in Table 1. The Reynolds number $Re = U_0 D / \nu$ is based on jet diameter D and its centerline velocity U_0 at the nozzle exit plane. The Mach number is $M = 0.9$. A near top-hat velocity profile with a tanh bounding shear layer was specified at the inflow plane. Small-amplitude, random fluctuations were imposed on the shear layer alone. Simulations A and B are at $Re = 11000$, but for different domain sizes—axial distances of $30D$ and $70D$, but with approximately the same grid spacing. Bogey and Bailly [13] have simulated a round jet for $75D$ at these conditions ($Re = 11,000$, $M = 0.9$). Cases C and D are at the much higher Reynolds number of 1.1 million. Spatial differences were obtained with a 6th-order compact scheme, and a 10th-order filter was applied to conserved variables after every time-step. Filter response functions are those in Fig. 3. Time-stepping is with a 2nd-order, explicit, Runge-Kutta scheme. Non-reflecting boundary conditions [21] were applied at the downstream and lateral boundary surfaces. The numerical method has been discussed in detail elsewhere [19]. An extensive discussion of the solution will also become available [22].

The Cartesian reference frame used is shown in Fig. 5; the x -axis was aligned with the jet and the origin is at the center of the jet on the inflow plane. The domain of interest is $0 < x < L_x$, $-L_y/2 < y < L_y/2$, $-L_z/2 < z < L_z/2$. The numbers of gridpoints in this region are also given in Table 1. Within this region, the grids were stretched in lateral directions outside a central square of side $1.5D$; grid spacing was increased in geometric progression by 1%. For cases B and D, the grid was stretched axially as well at 0.7%. The actual computational region was larger because a buffer zone was used near the downstream and lateral boundaries where the grid is stretched aggressively at 10%. There are additional gridpoints in these buffer zones, 30 in the axial and 20 in the lateral directions. Fine scale structures disappear in the buffer zone as they cannot be represented on the coarser grid.

An impression of the scale range is conveyed in Fig. 5 of iso-surfaces of vorticity magnitude from cases A and D. The larger scale range at the higher Reynolds number is evident. A sensitive test of the correctness of these solutions is the development of the inverse of the centerline velocity and the level of velocity fluctuations. The inverse of the centerline velocity is shown in Fig 6(a). For clarity, the curves for cases C and D have been offset upward by 3 units.

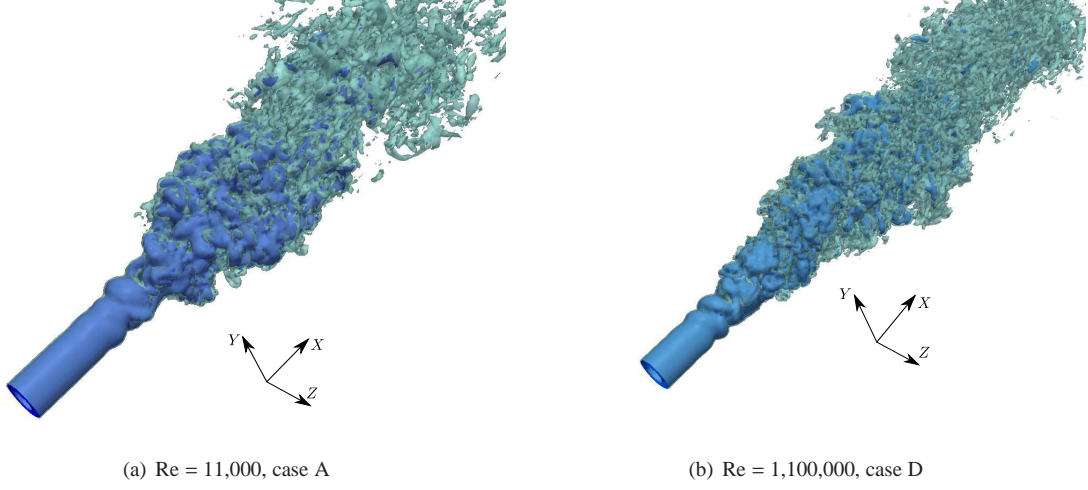


Figure 5: Isosurfaces of vorticity magnitude $\omega D/U_0 = 7.8, 15.6$.

The change in slope at $x/D \approx 10$ is the beginning of the turbulent portion. In all cases there is a clear linear range following breakdown. The curved portion near the downstream end is the from the outflow buffer region. Comparing cases A and B, we observe that, if the domain is extended, the slopes of these curves are essentially the same. Linear fit for case B over the portion $10 < x/D < 60$ has been included. The reciprocal B_u of the slopes linear fits for all cases are listed in table 1. The values for cases A, B and D are close to each other and agree closely with values from experiments (see, table 5.1 in [23]). For the coarse grid case C, the slope is significantly smaller. Incidentally, the curves for cases A and B also illustrate the correct effect of using a physical buffer layer: The solution for A departs from the solution for B only within its buffer layer.

Figure 6(b) shows the development of velocity fluctuations along the centerline, scaled with the local centerline mean velocity. For cases A, B and D, axial component u_{rms}/U_c tends to 0.24, and cross-stream components v_{rms}/U_c and w_{rms}/U_c to 0.18 as in experiments [24, 25]. Fluctuation levels are smaller for the coarse grid case C, and is consistent with the weaker decay rate of the centerline velocity (Fig. 6(a)). The grid employed for case C is inadequate, but on refinement (case D), an acceptable LES has been obtained.

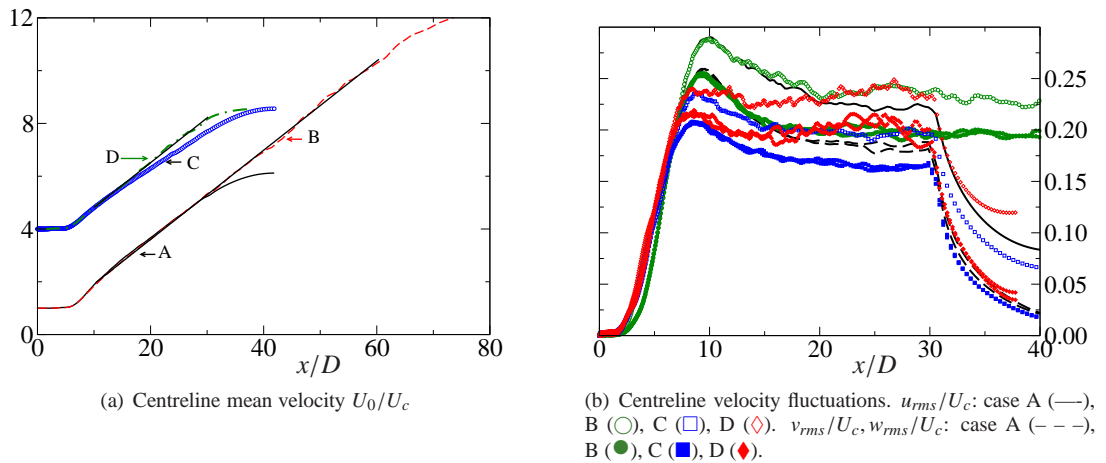


Figure 6: Streamwise development of jet. In (a), curves for cases C and D have been vertically offset by 3 units for clarity.

The time series of velocity components at many stations on lines $y = 0, z = 0$ (jet centerline) and $y = D/2, z = 0$

(jet boundary shear layer at inflow plane) were stored. Frequency spectra were calculated using the PWELCH function in MATLAB 8.6. Figure 7(a) shows frequency spectra of the streamwise velocity component, scaled with the local mean centerline velocity, $E(u)/U_c^2$ at $x/D = 4.99, 7.45, 9.96, 12.56$, and 14.94 from case A. Frequency f has been scaled with the jet half-radius $r_{1/2}$ and U_c . Close to the inflow plane the spectral range is small and solution field is fully represented and accurately computed on the chosen grid. Regular oscillations due to the vortex rings upstream of breakdown (see Fig. 5) can be observed as a low frequency peak in the spectrum at $x/D = 4.99$. Downstream this peak disappears as the flow breaks down to turbulence, and the spectrum broadens. Spectra collapse on these local scales to show self-preserving development for $x/D \geq 9.96$. Figure 7(b) shows spectra from cases A, C and D at $x/D \approx 12$. When the Reynolds number alone is changed, the spectra should extend to smaller frequencies as the inertial range extends, while the content at low frequencies should remain approximately the same (cases A and D). Clearly, the simulations support this expectation. When the grid is refined, the spectrum extends as smaller lengths and frequencies can be represented and computed accurately (cases C and D). Again, the changes are to the high frequency end of the spectrum, while the low frequency part of the solutions remains essentially the same.

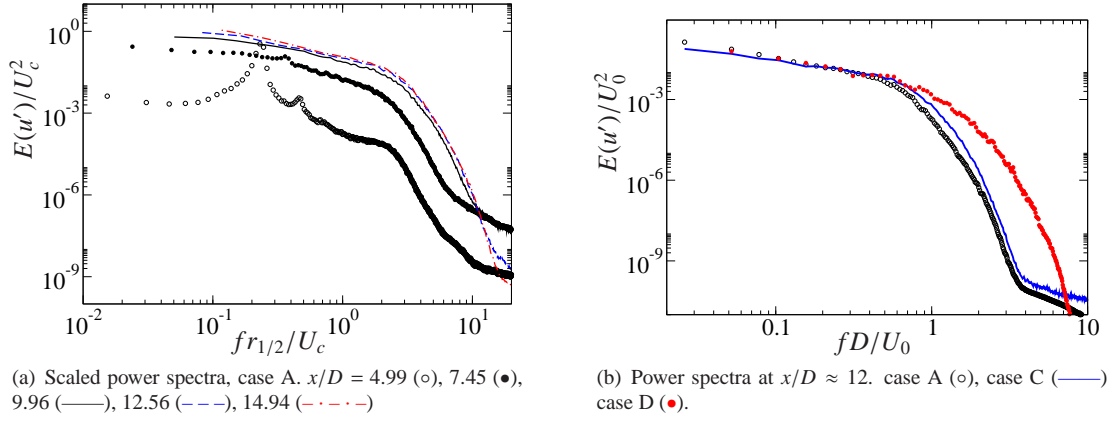


Figure 7: Power spectral density.

The analogy with use of outflow buffer regions can be taken a little further. Outflow buffer or sponge zone treatments are designed to continuously suppress fluctuations until simple conditions applied to a smoothed flow proves effective. If the change is abrupt at the interface between the region of interest and the buffer, the objective is not realized and problems appear at the interface. Filter response functions of explicit filters used in all the cases cited here fall off smoothly near the high wavenumber end as in Figs. 1, 2 or 3. If the explicit filter had a sharp cutoff at some $k_{\text{cutoff}} < k_{\text{max}}$, there would be energy accumulation near k_{cutoff} and the computations would diverge.

4. Other SGS models

With this understanding we can consider the effects of some other approaches.

The Smagorinsky SGS model is implemented as a term added to the momentum equations by setting the SGS stress tensor

$$\tau_{ij}^{\text{sgs}} = \nu^{\text{sgs}} S_{ij},$$

where S_{ij} is the strain rate tensor and ν^{sgs} is the eddy viscosity. The effect of this term is to damp *all* scales. Briefly, consider the 1-d equation (3) for the ‘LES’ variable \bar{u} . A Smagorinsky type model for \mathcal{R} would appear as

$$\frac{\partial \bar{u}}{\partial t} + \frac{\partial}{\partial x} f(\bar{u}) = \nu^{\text{sgs}} \frac{\partial^2 \bar{u}}{\partial x^2} \quad (9)$$

Here, for ease of illustration, let ν^{sgs} be a constant, though in the Smagorinsky model it is proportional to a measure of the local strain rate tensor. On taking the Fourier transform of equation 9, and Euler forward time-stepping, we can

write

$$\hat{u}(k, t + \Delta t) = \hat{u}(k, t) - \Delta t(ik\hat{f}) + \Delta t \nu^{\text{sgs}} k^2 \hat{u}(k, t).$$

Combining the 1st and 3rd terms on the rhs is equivalent to applying a filter with response function $\hat{G}_S = 1 - \Delta t \nu^{\text{sgs}} k^2$ to the solution at t . This filtering provides the SGS modeling. Although high wavenumber content is damped more (increasing as k^2), *all* content is damped. This is not to be considered a wrong model, because the damping of any fixed range of low wavenumber content will reduce as the grid is refined, but is, therefore, a less efficient model. When the dynamic Smagorinsky SGS model is applied, ν^{sgs} is determined during the course of the computation from the solution. The calibration coefficient that appears in the expression for ν^{sgs} varies with position and time. When

$$< \nu_{\text{Dynamic Smagorinsky}}^{\text{sgs}} > \leq \nu_{\text{Smagorinsky}}^{\text{sgs}}$$

suffices for stable computations, one can think of the dynamic model as applying a mean ν^{sgs} that is less than the standard model, and thereby offering a better solution due to the smaller damping of large scales.

The explicit filtering method described above has been called an implicit LES (ILES) method, perhaps, because the numerical method was designed for accuracy and stability and not explicitly for LES [26]. An earlier method called MILES had also been characterized as an ILES. Boris [27] had explained the effectiveness of MILES by stating, “monotone convection algorithms designed for positivity and causality, in effect have a minimal LES filter and matching subgrid model already built in. [This ensures] efficient transfer of the residual subgrid motions, [...] off the resolved grid with minimal contamination of the well-resolved scales by the numerical filter.” These features turn out to be requirements that appear in the derivation of the explicit filtering method. A variety of experiences with MILES, including an historical account, are available [28]. One way to understand the success of MILES is to recall that in the FCT algorithm, the anti-diffusive step is constructed from the local solution, and limited, to ensure that no new extrema are created. The FCT algorithm was designed to obtain higher-order flow fields, capturing shocks without oscillations. It proves effective as an algorithm for LES because it suppresses oscillations that will appear as nonlinear terms generate content at wavenumbers larger than the ones that can be represented on the chosen grid. In its treatment of the difficulty at the high wavenumber end, the algorithm is also optimal because it is designed to just prevent the appearance of new extrema based on the local state. Away from locations where the integration would not produce a new extremum, there is no modification of the solution. The implied filter is then active in a high wavenumber spectral buffer. Since MILES was found to be useful for LES without any explicit SGS model terms, the basic numerical method remained of relatively low order—FCT is 2nd-order in space. On discovering that a compact scheme with a high-order filter delivers useful LES without adding SGS model terms, Visbal et al. [26] have termed their method an ILES also. The explicit filtering methods cited here no longer attempt to provide any kind of dynamic, optimal filtering. Attempts in this direction did not reveal any significant benefit by changing the filter cutoff, or by reducing the frequency of its application. For secondary filtering (to be discussed below), the solution was not found to have any sensitive dependence on the secondary filter parameter.

4.1. Secondary filtering

Adams [5] had added a low-order relaxation regularization term to the differential equation for the LES field. In Stolz and Adams [4], this was briefly mentioned as the use of a secondary filter that improved the solution, but results were not included pending further investigation. It has been added and discussed in detail subsequently [6, 29]. When this term is added, the model eqn. 5 would be modified to read

$$\frac{\partial \bar{u}}{\partial t} + G * \frac{\partial f(Q * \bar{u})}{\partial x} = -\chi(I - Q * G) * \bar{u}. \quad (10)$$

Here, χ is a free parameter. Stolz et al. [6] found solutions to have but a weak dependence on χ . Mean velocity profiles showed very little difference as χ was changed by a factor of 8. As stated in Stolz et al. [6], the effect of adding this relaxation term can be realized by integrating without the additional term and filtering the field \bar{u} with filter QG every $1/(\chi\Delta t)$ timesteps. Or, that applying the filter QG to field \bar{u} every m timesteps while integrating eqn.5 is equivalent to integrating eqn. 10 with $\chi = 1/(m\Delta t)$. If $m = 1$, relaxation regularization is realized by applying the resultant filter $E * E = G * Q * G * Q$ to the evolving field. For flat filters of the type shown in Figs. 1 or 2, $E(\alpha_1) * E(\alpha_1)$ can be approximated by applying filter $E(\alpha_2)$, with α_2 slightly less than α_1 . So, a formal secondary filtering step and the distinguishable benefit that would accrue are not evident.

Acknowledgments

I thank my students Dr. S Chakravorty and Mr. Sumit Patel who provided data from their simulations for the discussions in § 3.

References

References

- [1] P. Sagaut, Large eddy simulation for incompressible flows, 3rd ed., Springer, 2006.
- [2] J. Mathew, H. Foysi, J. Sesterhenn, R. Friedrich, An explicit filtering method for large eddy simulation of compressible flows, *Physics of Fluids* 15 (2003) 2279–2289.
- [3] T. S. Lund, The Use of Explicit Filters in Large Eddy Simulation, *Computers and Mathematics with Applications* 46 (2003) 603–616.
- [4] S. Stolz, N. A. Adams, An approximate deconvolution procedure for large-eddy simulation, *Physics of Fluids* 11 (1999) 1699–1701.
- [5] N. A. Adams, Advances in direct deconvolution modeling of subgrid-scales for flows with discontinuities, in: CTR Annual Research Briefs 1999, Stanford University, 1999, pp. 317–327.
- [6] S. Stolz, N. A. Adams, L. Kleiser, An approximate deconvolution model for large-eddy simulation with application to incompressible wall-bounded flows, *Physics of Fluids* 13 (2001) 997–1015.
- [7] B. J. Geurts, Inverse modeling for large-eddy simulation, *Physics of Fluids* 9 (1997) 3585.
- [8] J. A. Domaradzki, E. M. Saiki, A subgrid-scale model based on estimation of unresolved scales of turbulence, *Phys. Fluids* 9 (1997) 2148.
- [9] M. Germano, U. Piomelli, P. Moin, W. H. Cabot, A dynamic subgrid-scale eddy viscosity model, *Phys. Fluids* 3(7) (1991) 1760–1771.
- [10] M. R. Visbal, D. V. Gaitonde, High-order-accurate methods for complex unsteady subsonic flows, *AIAA Journal* 37 (1999) 1231–1239.
- [11] M. R. Visbal, D. P. Rizzetta, Large-Eddy Simulation on curvilinear grids using compact differencing and filtering schemes, *ASME J. Fluids Engg.* 124 (2014).
- [12] S. Chakravorty, On large eddy simulation of reacting flows using the explicit filtering method with a filtered mass density, Phd thesis, Indian Institute of Science, 2010.
- [13] C. Bogey, C. Bailly, A family of low dispersive and low dissipative explicit schemes for flow and noise computations, *Journal of Computational Physics* 194 (2004) 194–214.
- [14] S. Chakravorty, J. Mathew, A high-resolution scheme for low Mach number flows, *Int. J. Num. Meth. Fluids* 46 (2004) 245–261.
- [15] J. Mathew, H. Foysi, R. Friedrich, A new approach to LES based on explicit filtering, *International Journal of Heat and Fluid Flow* 27 (2006) 594–602.
- [16] R. Hixon, E. Turkel, Compact Implicit MacCormack-Type Schemes with High Accuracy, *Journal of Computational Physics* 158 (2000) 51–70.
- [17] S. K. Lele, Compact Finite Difference Schemes with Spectral-like, *Journal of Computational Physics* 42 (1992).
- [18] S. Ganesh, Flow and sound field of free and impinging jets from LES using explicit filtering method, Phd thesis, Indian Institute of Science, 2013.
- [19] S. K. Patel, J. Mathew, Large Eddy Simulation of Supersonic Impinging Jets by adaptive, explicit filtering, in: 22nd AIAA Computational Fluid Dynamics Conference, Paper No. AIAA-2015-2298.
- [20] K. W. Thompson, Time dependent boundary conditions for hyperbolic systems, *Journal of Computational Physics* 68 (1987) 1–24.
- [21] T. Poinso, S. K. Lele, Boundary conditions for direct simulation of viscous flows, *Journal of Computational Physics* 101 (1992) 104–129.
- [22] S. K. Patel, Aeroacoustics of supersonic jets impinging on wedge deflectors from LES, Phd thesis, Indian Institute of Science, under preparation.
- [23] S. B. Pope, *Turbulent Flows*, Cambridge University, 2000.
- [24] N. R. Panchapakesan, J. L. Lumley, Turbulence measurements in axisymmetric jets of air and helium. part 1. air jet, *J. Fluid Mech.* 246 (1993) 197–223.
- [25] H. J. Hussein, S. P. Capp, W. K. George, Velocity measurements in a high-reynolds-number, momentum-conserving, axisymmetric, turbulent-jet, *J. Fluid Mech.* 258 (1994) 31–75.
- [26] M. R. Visbal, P. E. Morgan, D. P. Rizzetta, An implicit LES approach based on high-order compact differencing and filtering schemes, in: 16th AIAA CFD Conference, pp. Paper AIAA–2003–4098.
- [27] J. P. Boris, On large eddy simulation using subgrid turbulence models, in: J. L. Lumley (Ed.), *Whither Turbulence? Turbulence at the crossroads*, Springer, 1990.
- [28] F. F. Grinstein, L. G. Margolin, W. J. Rider (Eds.), *Implicit large eddy simulation*, Cambridge University, 2007.
- [29] S. Stolz, N. A. Adams, L. Kleiser, The approximate deconvolution model for large-eddy simulation of compressible flows and its application to shock-turbulent-boundary-layer interaction, *Physics of Fluids* 13 (2001) 997–1015.